Planetary and Space Science 278–279 (2026) 106295

Contents lists available at ScienceDirect

Planetary and Space Science

journal homepage: www.elsevier.com/locate/pss

The role of basal heating in lubricating icy landslides in the Solar System

Andrea Caccia [a,*], Fabio V. De Blasio [a], Ludovica Dalla Costa [a], Biagio Di Mauro [b], Giovanni B. Crosta [a]

[a] Department of Earth and Environmental Sciences, University of Milan-Bicocca, Milan, Italy
[b] Institute of Polar Sciences, National Research Council, Milan, Italy

A B S T R A C T

A significant number of the major celestial bodies in the Solar System are characterized by high percentages of ice in their surface composition. Previous works have shown how the rheological behavior of ice-rock mixtures under different pressure, gravity and temperature conditions can be studied based on the morphologies of landslides. It has long been known that terrestrial landslides that occur on frozen surfaces show very low apparent friction, calculated as the aspect ratio between the fall height of the landslide and its horizontal movement. A possible mechanism to explain this low friction and consequently high mobility is the presence of a temporary meltwater layer at the interface between the debris and the impacted ground. This paper examines landslides on different planetary bodies of the Solar System composed of ice in varying amounts, from the ones containing ice only in the rock pores, to nearly completely icy mass flows.

A mechanical-thermodynamic model of ice melting at the base of these landslides is investigated. Lubrication is explicitly introduced as a consequence of frictional melting of ice, which is found to be very sensitive to the gravity field, the topographic profile, and the temperature of the bodies. Results explain the decrease in friction coefficient, while the volume effect is seen to occur with more efficacy for bodies with high gravity and is absent for the very low-gravity comet 67/P. The results indicate the importance of initial temperature, ice content and especially gravity in ice lubrication dynamics of icy landslides in the different planetary bodies.

1. Introduction

Water ice has been observed to be extremely abundant in the Solar System (Encrenaz, 2008) and its dynamics strongly influence the geological processes occurring on the celestial bodies with a large percentage of it in their composition (Bulmer, 2012). In addition, one of the interests in these cold, devoid of liquid water, highly radiated and poor in nutrients environments lies in the fact that under such conditions, life has been observed to thrive on Earth (Anesio et al., 2017; Rozwalak et al., 2022). This observation raises the question of whether life, in any form, could be present on other icy worlds (Khuller et al., 2024).

Landslides have been observed to occur throughout the Solar System (Bulmer, 2012) on bodies of extremely diverse nature. Aside from Earth, landslides occurred on Mercury (Brunetti et al., 2015), Venus (Malin, 1992), the Moon (Scaioni et al., 2018), Mars (Lucchitta, 1987; McEwen, 1989; Quantin et al., 2004; Lucas et al., 2014; Crosta et al., 2018a; Pajola et al., 2022; Guimpier et al., 2022), Martian moon Phobos (Shingareva and Kuzmin, 2001), large asteroids Vesta and Ceres (Otto et al., 2013; Schmidt et al., 2017), Jovian moons (Schenk and Bulmer, 1998; Moore et al., 1999), Saturn moons (Singer et al., 2012), Pluto's moon Charon (Beddingfield et al., 2018, 2020) and comet 67P/Churyumov-Gerasimenko (Lucchetti et al., 2019). While some landslides have been observed in worlds devoid of ice (for example Mercury, Io, the Moon, Phobos), others are affected by ice or are nearly completely icy (for example on Earth, Mars, Callisto, Ceres, Iapetus, Charon).

Landslides have extremely variable morphologies that are related to the characteristics of the planetary body on which they occur (Table 1). The main factors that play a role in the development of these structures on icy worlds are the properties of the surface and landslide materials (rheology and quantity of volatiles), the collapse dynamics, the local topography and, most importantly, the gravitational acceleration of the terrestrial body. Based on the analysis of the morphology of the landslides and considering all the different properties of the planet on which they occurred, it is therefore possible to gain insight into ice in the icy bodies of the solar system by studying the behavior of the mass emplacement.

Several authors have shown (initially for Earth, and then for Mars and other planetary bodies) that the effective friction coefficient defined as the ratio H/L between the fall height H and the runout L of the landslide decreases drastically with the volume, which is also called the volume effect (Scheidegger, 2012; Shaller, 1991; Bulmer, 2012; Crosta et al., 2018). Note that following common usage in landslide research (e.g., Scheidegger, 1973) we shall be using the volume of the landslides, even though it is the mass that plays the role in the dynamics. This difference is relatively small considering that the density changes little

* Corresponding author.
E-mail address: a.caccia7@campus.unimib.it (A. Caccia).

https://doi.org/10.1016/j.pss.2026.106295
Received 19 June 2025; Received in revised form 27 April 2026; Accepted 29 May 2026
Available online 1 June 2026

among the different rock types, while the volume changes by several orders of magnitude. The volume effect, however, is not exhibited by all celestial bodies in the same way, and in particular not in the observed and modeled data for comet 67P, where the effective friction of landslides is approximately the same regardless of the volumes involved (Lucchetti et al., 2019). There are several hypotheses (e.g. acoustic fluidization, Collins and Melosh, 2003; Flash-heating, Lucas et al., 2014) but no accepted explanation for the volume effect, even though it appears that ice and water may be involved (e.g., De Blasio, 2009). In trying to understand this behavior, we study landslides on a considerable number of planetary bodies that show significant percentages of ice in their composition (Brunetti et al., 2015; Malin, 1992; Scaioni et al., 2018; Lucchitta, 1987; McEwen, 1989; Quantin et al., 2004; Lucas et al., 2014; Crosta et al., 2018b; Shingareva and Kuzmin, 2001; Otto et al., 2013; Schmidt et al., 2017; Schenk and Bulmer, 1998; Moore et al., 1999; Singer et al., 2012; Beddingfield et al., 2018; Lucchetti et al., 2019; Beddingfield et al., 2020) and are covered by extensive data that allows to run morphological analyses. We focus our work on the bodies of Mars, Ceres, Callisto, Iapetus, Rhea, Charon, comet 67P/Churyumov-Gerasimenko and Earth, the last to use as a comparison (Fig. 1). Throughout this study, the terms "icy" and "ice" refer to landslides composed by less than 70% ice and more than 70% ice, respectively.

On Earth, icy landslides occur mostly in mountain environments (Fig. 1a–h). They produce lobate, elongated deposits usually showing furrows on the surface parallel to the flow direction. Similar morphologies can be found on Mars (Fig. 1b), where the volumes of material involved are significantly larger, resulting in massive debris aprons with evident furrows on their surface. Valles Marineris region shows great abundance of such morphologies (Crosta et al., 2018a). On other planetary bodies (Fig. 1c and d,e) landslides are typically found within the structure of ancient impact craters, as their rims can be extremely steep and unstable. On Comet 67P/Churyumov-Gerasimenko (Fig. 1g), the volumes of materials involved are significantly lower than all the other cases studied and no elongated debris aprons or furrows have been observed, seemingly implying that the extremely ice-rich landslide material assumes morphologies typical of rock falls on this body (Lucchetti et al., 2019).

This work aims to give an overview and analysis of the icy landslide phenomenon throughout the Solar System, where ice persists at different ranges of pressure and temperature (Petrenko and Whitworth, 1999). The purpose is to provide the main factors influencing these events and to relate them with the morphological characteristics that these structures assume on the different planetary bodies. Through the usage of thermodynamic modelling, we tested the hypothesis that the generation of a meltwater layer at the interface between the surface and the detached material may explain the mobility and volume effect in icy landslides.

2. Methods

2.1. Landslide data acquisition

Data for this study was collected from planetary landslide databases. The ratios H/L (fall height divided by runout distance, of particular relevance for landslide studies) for Ceres and Charon were obtained by the dataset of missions DAWN (Russell and Raymond, 2012) and New Horizons (Guo and Farquhar, 2008) respectively, accessible through JMARS software (Christensen et al., 2009). We found our results consistent with the works of Schmidt et al. (2017) on Ceres and Beddingfield et al. (2018) on Charon. We acquired images and H/L values for Earth and Mars landslides from the work of Crosta et al. (2018a) and the same data for comet 67P/Churyumov-Gerasimenko from Lucchetti et al. (2019). Most of the data for Mars were collected by MRO mission (Zurek and Smrekar, 2007). Extremely valuable morphological images over the bodies of Rhea, Callisto and Iapetus were provided by CASSINI mission (Lebreton and Matson, 1992) and collected in the work of Singer et al. (2012).

2.2. Basal heating model

Frictional heat is known to produce a self-lubrication layer in icy materials dramatically decreasing ice friction. In laboratory conditions, the phenomenon has been assessed in numerous conditions of temperature, speed, pressure, and roughness (e.g., Colbeck, 1988; Petrenko and Whitworth, 1999; Maeno et al., 2003; Kietzig et al., 2010). However, in the more remote and inhomogeneous conditions under landslide bodies, the dynamics of lubrication are still a matter of investigation.

The model described here is a modification of the one proposed by De Blasio (2014) and Crosta et al. (2018a) to estimate the amount of water melted at the base of a terrestrial or a Martian rock avalanche and the consequent lubrication at the base. This model does not introduce

Table 1
General characteristics of the examined planetary bodies. As Average temperature we assume the temperature of the body averaged between its lowest and highest values. The terms "icy" and "ice" refer to landslides composed by less than 70% ice and more than 70% ice, respectively.

	Equatorial radius (km)	Average gravity (m/s^2)	Main surface lithologies	Average density (kg/m3)	Ice fraction ϵ	Mass (kg)	Average Temperature (K)
Comet67P	2	2.2x10^{-4}	Ice and Dust (Filacchione et al., 2019a,b)	530 (Pätzold et al., 2016)	0.99	1x10^{13}	170
Iapetus	735	0.223	Roughly ¼ of Carbonatic Chondritic Rocks and ¾ of Ice (Clark et al., 2012)	1083 (Thomas et al., 2007)	0.95	1.806x10^{21}	100
Ceres	487	0.28	An inner core of chondritic material with an outer layer of ice covered by a silicate layer. (Rivkin et al., 2012; King et al., 2018)	2170 (McCord and Sotin, 2005)	0.2	9.28x10^{20}	200
Rhea	763,5	0.26	An inner rocky core with an ice-rock mantle and an icy surface (Anderson and Schubert, 2007)	1236 (Thomas et al., 2007)	0.95	2.306 x10^{21}	99
Callisto	2410	1.236	Rock and ice mixture in almost equal quantities. (Moore et al., 2004)	1834 (Anderson et al., 2001)	0.4	1.076 x10^{23}	134
Charon	606	0.288	Ammonia hydrates and water ice (Protopapa et al., 2021)	1705 (Spencer et al., 2021)	0.45	1.589 x10^{23}	53
Mars	3402	3.69	Igneous and sedimentary rocks with a varying percentage of subsurface ice (Taylor, 2013)	3934 (Smith et al., 1999)	0.2 [a]	6.42x10^{23}	220
Earth	6378	9.81	Basaltic, granitic, metamorphic and sedimentary rocks. In most cases, water or ice are present in the landslide (McDonough and Sun, 1995)	5514 (Williamson and Adams, 1923)	0.2 [b]	5.97x10^{24}	260

[a] Assumed based on morphological analysis.
[b] In glaciated landslides (Schneider et al. (2011)).

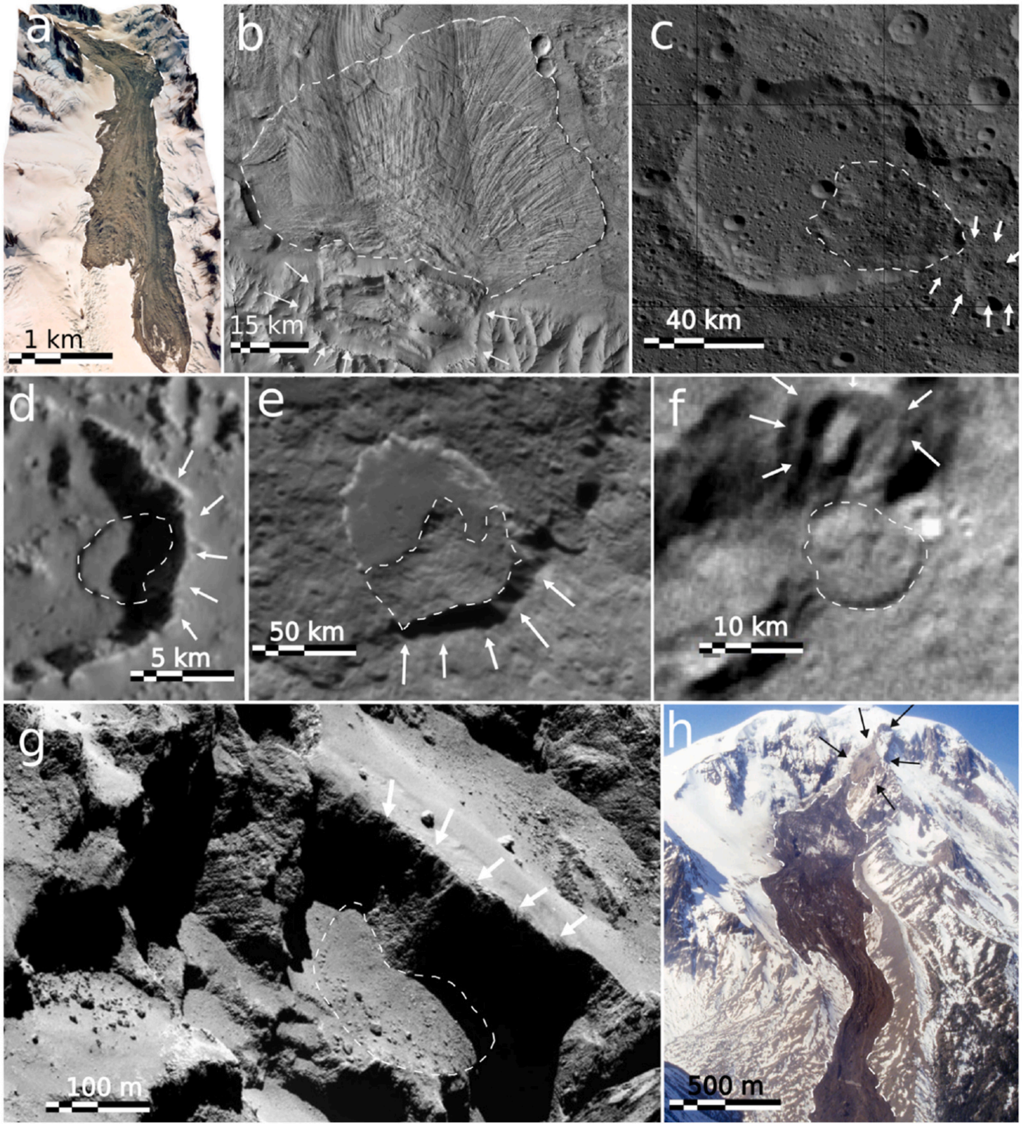

Fig. 1. Examples of landslides studied in this work and found on different planetary bodies. a) "icy" landslide on Earth (ice fraction 20%) located on Mount Munday, Canada. Data and picture from Sosio et al. (2012). b) Martian landslide "Coprates Labes". CTX image. c) landslide within Darzamat crater on Ceres. DAWN mission image. d) landslide on Callisto located at 24.898 N, 218.295 E. Galileo mission image. e) landslide on Iapetus located within Malun crater. Cassini mission image. f) landslide on Charon located at 21.25 N, 198.5 E. New Horizons mission image. g) landslide on Comet 67P Churyumov-Gerasimenko, note that the scale is extremely lower than the other bodies. Image ID: N20141112T164351560ID30F22. Image from Rosetta mission. h) "ice" landslide on Earth (ice fraction 80%), Schneider et al. (2011) located on Mount Adams, Washington, USA. Image credit: USGS. In each image the debris aprons are highlighted by the dashed line and the arrows indicate the detachment scarp. Images on Rhea were not available.

deformation, assuming that the landslide is represented as a rigid slab with thickness H_s that does not change shape during sliding. The basic hypothesis is as follows: a thicker landslide exerts more pressure at the base than a thinner one, resulting in more heat generated through friction. Consequently, the frictional heat increases the temperature of the basal ice until melting occurs. The resulting layer of water lubricates the base of the landslide (Fig. 2) and at the same time reduces the frictional melting. It is suggested that water produced in an icy landslide is rapidly consumed by refreezing, evaporation, or incorporation into the granular matrix when the motion stops.

Let us first consider the case of a landslide and of the sliding surface composed entirely of ice. At the base of the slab, the pressure is given by

$$P = \rho_{ice} g\, H_s \cos\beta \quad (1)$$

and the frictional force is

$$F = M\, g \cos\beta\, \mu = \rho_{ice} g\, H_s\, S \cos\beta\, \mu \quad (2)$$

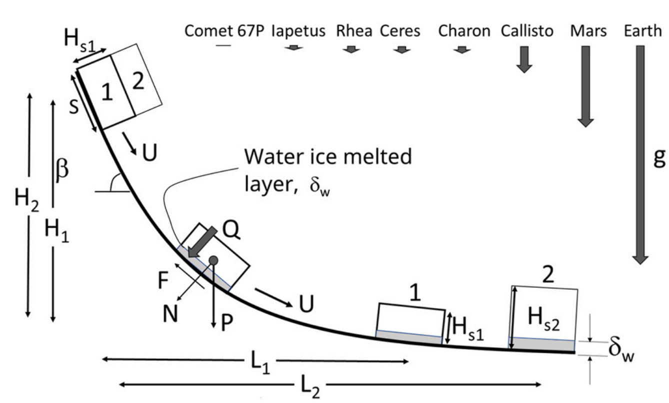

Fig. 2. Schematization of the sliding model used in this work. The lengths of g arrows are proportional to the gravity field on the specific planetary body.

where S is the surface area at the base of the slab, β is the local slope of the topography, g is the gravitational acceleration and μ is the friction coefficient.

The mechanical work dissipated at the base of the slab (in joules) over a time interval dt is (Crosta et al., 2018a)

$$dL = FUdt = \rho_{ice} g\, H_s\, S \cos\beta\, U\, \mu\, dt \tag{3}$$

where U is the velocity. Only one part of this work results in heating the interface between the slab and the ground, as some heat is carried away from the immediate contact zone (e.g. part is used in fragmentation, and in the generation of seismic waves). Therefore, the fraction e of work that contributes to the melting of water is:

$$dQ = e\, dL \tag{4}$$

The amount of melted water $d\,M_w$ in the same time interval dt is found by equating this heat with the amount of heat necessary to increase the temperature to the melting point of a mass dM of ice and then to melt it:

$$e\,\rho_{ice} g\, H_s\, S \cos\beta\, U\, \mu\, dt = (c\Delta T + \lambda)\, dM_w \tag{5}$$

where c, ΔT (>0), and λ are the specific heat, the temperature difference between the ice before melting and the melting point (i.e., the ice is initially at a temperature ΔT below zero), and the latent heat of fusion, respectively.

We can now rewrite $dM_w = \rho_{water} S\, \delta_w$, where δ_w is the thickness of water produced by the melting. Thus, the increase in water thickness over time is:

$$\frac{d\delta_w}{dt} = e\, \frac{g\, H_s \cos\beta\, \mu}{c\Delta T + \lambda}\, \frac{\rho_{ice}}{\rho_{water}} U \tag{6}$$

In laboratory conditions with pure ice, or when solid impurities are negligible, it is known that a water layer a few tens of microns thick can significantly reduce the friction of ice, explaining the slipperiness of ice at not too low temperatures (normally not lower than −35°C; Maeno et al., 2003; Kietzig et al., 2010; Colbeck, 1995). However, because rock fragments in a landslide have irregular surfaces, the thickness of the water layer must be much greater to achieve any form of lubrication (Crosta et al., 2018a).

In the model, which deals with impurity-rich ice, it is assumed that the critical thickness δ^* for lubrication is much greater than the tens of microns needed for pure ice and is at least in the order of the size of solid granules. Even this quantity is difficult to determine because the size of the clasts at the base of the landslide is itself determined by the fragmentation occurring during the collapse of the landslide.

We assume, in agreement with the model by Crosta et al. (2018a), that friction decreases according to

$$\mu = \mu_0 \exp\left(-\frac{\delta}{\delta^*}\right) \tag{7}$$

where δ^* is expected to be larger for icy conditions than for pure ice conditions and μ_0 is the dynamical friction coefficient in the absence of lubrication. The crucial point of the model explicit by Eq. (7) is that friction decreases as δ_w increases.

In the absence of air drag (which is certainly a good approximation for bodies with thin atmosphere and is valid even for Earth except for extreme speeds), the acceleration depends on the friction in a simple way:

$$\frac{dU}{dt} = g(\sin\beta - \mu\cos\beta) \tag{8}$$

If friction were constant, this model would be easily solvable for any slope profile. However, due to the complex behavior of friction modified by lubrication, the model needs to be solved numerically using the three equations described (6-8) $\frac{d\delta_w}{dt}$, μ and $\frac{dU}{dt}$, and with a plausible downslope sliding profile (slope topography) for the landslide. Here, we used an exponential profile for the topography of the form

$$y(x) = y_0 \exp\left(-\frac{x}{\Lambda}\right) \tag{9}$$

where x is the horizontal position of the landslide, Λ is a distance scale after which the elevation diminishes from an initial value of y_0 to $\frac{y_0}{e} \approx 0.368\, y_0$. The thickness of the landslide is assumed constant during sliding, and additionally the landslide is not lifted up by the underlying water later, a reasonable approximation since the fraction of ice removed from the base due to melting is much smaller than the thickness of the landslide itself (i.e. $\delta_w \ll H_s$).

If the landslide is composed partly of rock, the rest being ice, the equations are modified as follows. First, the pressure at the base will be higher because rock has a higher density. So instead of ρ_{ice}, we use $\rho = \epsilon\rho_{ice} + (1-\epsilon)\rho_{rock}$ where ϵ is the volume fraction of ice, and the pressure at the base becomes $P = \rho g\, H_s \cos\beta$. Another difference is that now only a fraction $\epsilon\rho_{ice}$ of the mass can melt. Finally, the specific heat of the mixture changes since the specific heat of rock is different from that of ice. Assuming that the heat generated by friction δQ is sufficient to heat a thickness of rock dh (with water ice inside) to the melting temperature of water ice, we get

$$\delta Q = [(c_{ice}\epsilon\rho_{ice} + c_{rock}(1-\epsilon)\rho_{rock})\Delta T + \lambda\epsilon\rho_{ice}]\, S\, dh \tag{10}$$

Putting together these modifications, we obtain

$$\frac{d\delta_w}{dt} = e\,\epsilon\, \frac{\epsilon\rho_{ice} + (1-\epsilon)\rho_{rock}}{\rho_{water}}\, \frac{H_s \cos\beta\, \mu}{[(c_{ice}\epsilon\rho_{ice} + c_{rock}(1-\epsilon)\rho_{rock})\Delta T + \lambda\epsilon\rho_{ice}]}\, U \tag{11}$$

There are two additional corrections to the model. The first concerns the possibility that some water is lost from the tail of the slab. We must thus include the length of the slab (which previously was not part of the model), denoted L_s. The amount of water lost per unit time is of the order $\frac{1}{2} U\, \delta_w\, W$, where W is the width of the slab (where it is assumed that the fluid velocity at the base and in contact with the slab are respectively 0 and U from which the factor $\frac{1}{2}$ is obtained by averaging). Dividing by the surface area of the slab, we obtain the rate of change of thickness due to loss from the tail $\frac{1}{2}\frac{U\delta_w}{L_s}$. The second correction concerns the case where the thickness of water becomes much greater than the asperities of the terrain. In this case, it is assumed that friction decreases significantly (as already observed), but the phenomenon of drag increases due to the turbulence in the water layer, which increases the resistance at the base of the landslide. The drag leads to a quadratic dependence of velocity through a drag coefficient C_D. The formula for drag resistance is discussed in greater detail in De Blasio (2014). Below are the final equations that account for these corrections and that are used in the simulations:

$$\frac{dU}{dt} = g(\sin\beta - \mu\cos\beta) - \frac{1}{2} C_D \frac{\rho_w}{\rho H_s}\left(1 - \exp\left(-\frac{\delta}{\delta^*}\right)\right) U^2 \tag{12}$$

$$U(t) = \int_0^t \frac{dU}{dt}\, dt \tag{13}$$

$$x = \int_0^t U(t)\, \cos\beta\, dt \tag{14}$$

$$\delta(t) = \int_0^t \frac{d\delta_w}{dt}\, dt \tag{15}$$

$$\sin\beta = \frac{|y'(x)|}{\sqrt{1 + y'(x)^2}} \tag{16}$$

$$\frac{d\delta_w}{dt} = e\ \epsilon\ \frac{\epsilon\rho_{ice} + (1-\epsilon)\rho_{rock}}{\rho_{water}} \frac{H_s\ \cos\beta\ \mu}{[(c_{ice}\epsilon\rho_{ice} + c_{rock}(1-\epsilon)\rho_{rock})\Delta T + \lambda\epsilon\rho_{ice}]} U - \frac{1}{2}\frac{U\delta_w}{L_s} \tag{17a}$$

$$\frac{d\delta_w}{dt} = e\ \frac{g\,H_s\ \cos\beta\ \mu}{c\Delta T + \lambda} \frac{\rho_{ice}}{\rho_{water}} U - \frac{1}{2}\frac{U\delta_w}{L_s} \tag{17b}$$

Where Eqs. (17a) and (17b) hold for mixed and pure ice avalanches, respectively.

The calculation method consists of integrating the equations of motion (11-17) numerically. The time variable is discretized with a time step of the order of 1 ms. At a given time step, Eqs. (12) and (11) are calculated and used to propagate the solution in time (for example, $U(t+\delta t) = U(t) + \left(\frac{dU}{dt}\right)_t \delta t$ where $\left(\frac{dU}{dt}\right)_t$ is calculated with the right hand side of Eq. (12) at time t, and then integrated again to find the position $x(t+\delta t)$ at time $t+\delta t$ as $x(t+\ \delta t) = x(t) + U(t)\delta t + (1/2)\left(\frac{dU}{dt}\right)_t \delta t^2$). Owing to the simplicity of the model, an Euler algorithm is sufficiently precise for the integration.

Note that for the case of Charon, since the volatile ices on the surface consist of a mixture of water ice (≈70%) and ammonia ice (≈30%) (Protopapa et al., 2021), the model was integrated with the effects of this mixture following the work of Hogenboom et al. (1997). The main changes in this model are variations in melting T, density, specific heat and latent heat of the ice mixture.

2.3. Parameters selection

While some parameters, such as the local slope, gravity and temperature are either well-known or can be reasonably assessed, others (Table 2) are more difficult to determine. A crucial quantity that is difficult to ascertain is the critical thickness δ^*, i.e., the critical thickness of the water layer needed to lubricate efficiently the landslide. This parameter is strongly dependent on the roughness of the terrain and the grain dimensions. We therefore proceeded empirically and ran a series of simulations varying this parameter, with unrealistically low and high values as endmembers ($\delta^* = 0.0001 - 1m$), in order to find the value capable of better reproducing the observed morphologies (Fig. 3). The figure shows, next to each legend entry, the level of accuracy for each curve. This was evaluated by comparing measured H/L values with those predicted from the modeled volume–H/L relationships. The misfit was then quantified as the absolute vertical deviation in log-space, $r = \left|\log_{10}(H/L)_{\text{obs}} - \log_{10}(H/L)_{\text{model}}\right|$, which represents a multiplicative error. This was converted into a percentage accuracy defined as $\text{Accuracy} = 100 \times 10^{-r}$, such that perfect agreement corresponds to 100%, and deviations reflect the factor by which modeled and observed values differ. The overall performance of each curve was then quantified as the mean accuracy across all data points.

We ran these simulations for the case of Mars, where a large inventory of data was available. From this study, we found that a value of $\delta^* = 0.01\ m$ (1 cm) provides a reasonable approximation to model this lubrication. We chose to use a single value for this parameter for all the planetary bodies since, as displayed by Fig. 3, it does not introduce significant errors; large variations of even 1 order of magnitude within δ^* have been observed to provide values within acceptable ranges, although less accurate.

Another difficult parameter to set is the efficiency e, that is, the fraction of the mechanical energy dissipated by the landslide ending up as thermal energy and raising the temperature at the base of the mass movement. The distribution of dissipated energies in ice-rich landslide phenomena has been little addressed in the literature (De Blasio et al., 2018). In the calculations, an empirical approach was therefore used, simply adjusting the parameter until convergence with the empirical data was found. Fig. 3 also displays the results for these simulations, which show the best fit for the case of $e \approx 0.1$ (10%). Similarly to δ^*, we applied a single value of e to all our simulations since it has been observed that even large and unrealistic values (i.e. e = 0.5) still provide data that, although less accurate, still fall within the observed morphologies.

2.4. Profiles and volumes used for the modelling

The profiles shown in Fig. 4 were obtained after calculating the average height H of the landslide scarp for each celestial body and subsequently applying an exponential decrease in the topography. The slope profile of the landslides follows the exponential law $y(x) = y_0\ exp\left(-\frac{x}{\Lambda}\right)$. The values for each planet are displayed in Table 3.

The modeled volumes, on the other hand, have been obtained following the empirical law:

$$V = H_S L W = H_S{}^*(sH_S)^*(jH_S) \tag{18}$$

where H_S is the thickness of the moving slab, L is the maximum length reached by the moving slab, W is the maximum width reached by the moving slab, s and j are scaling factors based on empirical observations (empirical aspect ratios, Li et al., 2022) equal to 10 and 20, respectively, and which assume that width and length scale linearly with thickness.

3. Results

The results of the simulations are presented in Fig. 4 in three columns for each planetary body. From the first to the third column, the data reported are the thickness of the lubricating water layer δ_w as a function of the distance travelled by the slab paired with the profile modeled for the simulation (see Supplementary Materials for enhanced representation of the profiles), the velocity of the slab as a function of the horizontal distance travelled, and the friction coefficient μ as a function of the horizontal distance travelled. Each simulation for every planetary body was run 10 times with a constant increase in the slab thickness (ΔH_s) between each simulation, using as starting point a value that would reproduce the lowest landslide volume recorded by data on each planetary body (values shown in Fig. 4 under each planet's name). Table 1 shows the values of g, T and ϵ used for each planetary body.

Note that for each body, and given a certain slab thickness, the speed shown in the second column initially increases, rapidly reaching its peak in the first third of its path, and then decreases more gently until it drops to zero. However, both the maximum speed and the final position of the slab increase with the slab thickness. This behavior is related to the results presented in the first column of Fig. 4, where the thickness of the lubricating water layer δ_w is shown as a function of the distance travelled by the slab. In this column, it is possible to appreciate how an increase in slab thickness H_s is followed by an increase in the water layer thickness δ_w. This result leads to the counter-intuitive outcome that a thicker slab

Table 2
Values of key parameters kept constant in the simulation.

Parameter	δ^* (m)	C_D	e	μ_0	λ (J/kg)	c_{rock} J/(kg K)	c_{ice} J/(kg K)	$c_{ice} + NH_3$ J/(kg K)
Value	0.01	0.5	0.1	tan(40°) = 0.839	330,000	1230	1880	1736

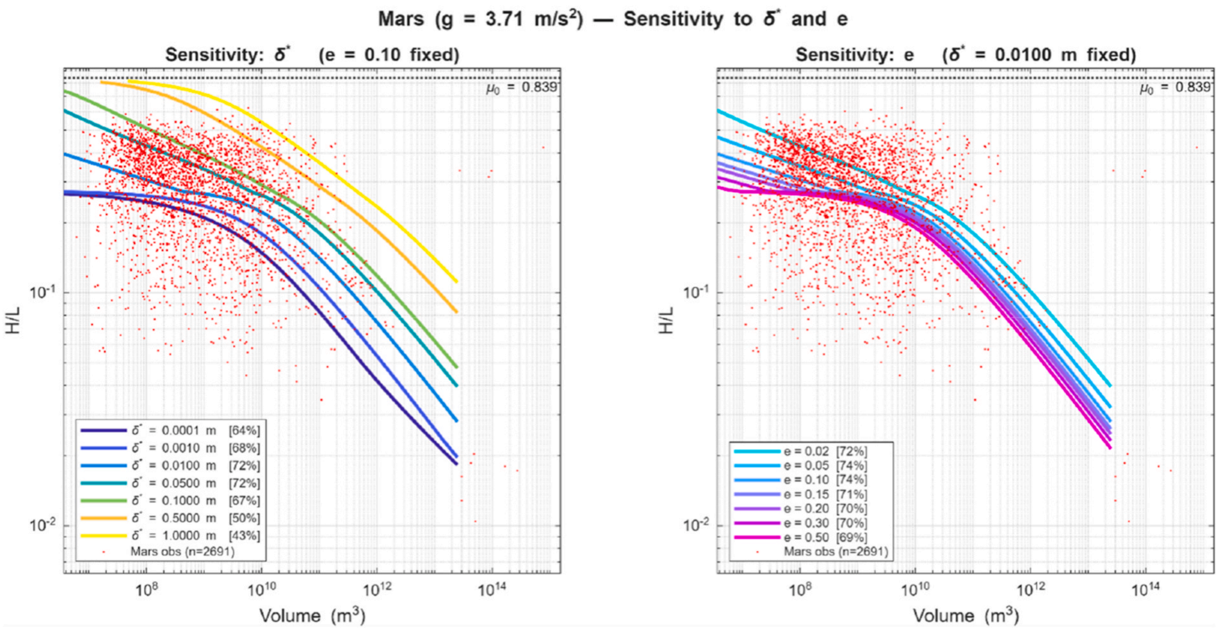

Fig. 3. Simulations for the Martian case varying the parameters of e and δ^*. Each curve refers to a different simulation ran with the respective parameters; red dots are the measured data from optical imagery on Mars. In the legend, next to each curve we displayed the level of accuracy between the curve and the measured data. Left: H/L-volume simulated by varying values of δ^*. Right: H/L-volume simulated by varying values of *e*. (For interpretation of the references to colour in this figure legend, the reader is referred to the Web version of this article.)

(corresponding to a larger landslide volume) is more efficient in reducing the friction compared to a thin one. The friction coefficient as a function of the runout distance L is shown in the third column of Fig. 4. Each line of Fig. 4 corresponds to one simulation cycle, and the columns show different aspects of the same simulation within the same line. Note that the friction coefficient decreases with an increase in lubricating water thickness δ_w and slab velocity. Thus, the results indicate that the pressure exerted by the travelling mass has a major role in defining the friction applied at the base of the landslide and consequently the amount of meltwater produced, the velocity of the slab (which increases as the frictional force decreases), and the total distance travelled by the landslide itself

Noteworthy are the results obtained for the Comet 67P Churyumov-Gerasimenko, ice case ($\epsilon \approx 1$). Here, regardless of the pressure applied to the underlying layers, the weak gravitational field nullifies the volume effect, preventing the formation of any lubricating layer ($\delta_w = 0$). *A* s a consequence, the friction coefficient does not decrease and only one single line is visible in the three graphs since all the different results with increasing slab thickness collapse to the same line. This effect results in the high H/L values observed for the case of the Comet (Lucchetti et al., 2019). On the other hand, the case of Earth, when compared to Ceres' results (comparable landslide volumes), shows that a difference of roughly 9 m/s^2 in the gravitational acceleration results in up to two orders of magnitude difference in friction coefficients.

Lastly, note that some of the velocity plots in the second column of Fig. 4, and in particular most curves for Mars and the ones at high speed for the Earth, Iapetus, and Charon, are convex for some values of the horizontal position x. Mathematically, this occurs when the second derivative of the velocity with respect to the position becomes positive, a condition occurring when the drag term (second term on eq. (12)) becomes important. The convexity is thus due to the growing importance of the drag resistance versus friction for fast landslides.

4. Discussion

4.1. Plot of H/L versus volume

Fig. 5a, reporting the H/L ratios calculated with the model vs volume of the landslide, summarizes the results of the simulations. The values for the volumes of the observed landslides (stars in Fig. 5a) have been obtained from the literature (Crosta et al., 2018a;Schmidt et al., 2017; Moore et al., 1999; Singer et al., 2012; Beddingfield et al., 2018; Lucchetti et al., 2019). The accuracy of each fitting can be found in Fig. 5c, which shows the model performance for each measured volume in Fig. 5a. This accuracy was calculated as described in section 2.3.

The curves in Fig. 5a and b are the results from hypothetical modeled landslides on the respective body. H/L, also known as Heim's ratio, is here used as a proxy for μ (Heim, 1882). Note that the H/L ratios for most of the calculated landslides tend to decrease with simulated volume, possibly indicating a general trend common to icy planets for the volume effect. Moreover, the slope of the curves changes with volume and each body shows a characteristic "knee" (diamond markers in Fig. 5a), followed by an asymptotic tendency to a constant slope (shown next to each curve) for the highest volumes. We investigated this behavior and found it to be strictly linked to the position of arrest of the simulated landslide along the slope profile (See Fig. 4 and Supplementary Materials for additional information). While at lower volumes the landslide stops along the slope without reaching the horizontal surface, larger landslides travel further to a point in which H remains constant for increasing L so that the ratio H/L decreases faster. Thus, the knee in the H/L curves occurs when the landslide volume is sufficient to bring it from the initial steep incline to the horizontal part of its path.

4.2. Driving factors in basal melting

What changes drastically between the different simulations is the value of H/L for a given volume. For example, the H/L curve for Mars at any given volume is higher than the one for Earth. Similarly, the simulated curve for Charon is higher than the one for Mars, and the one for Iapetus is the highest, except for the comet 67P.

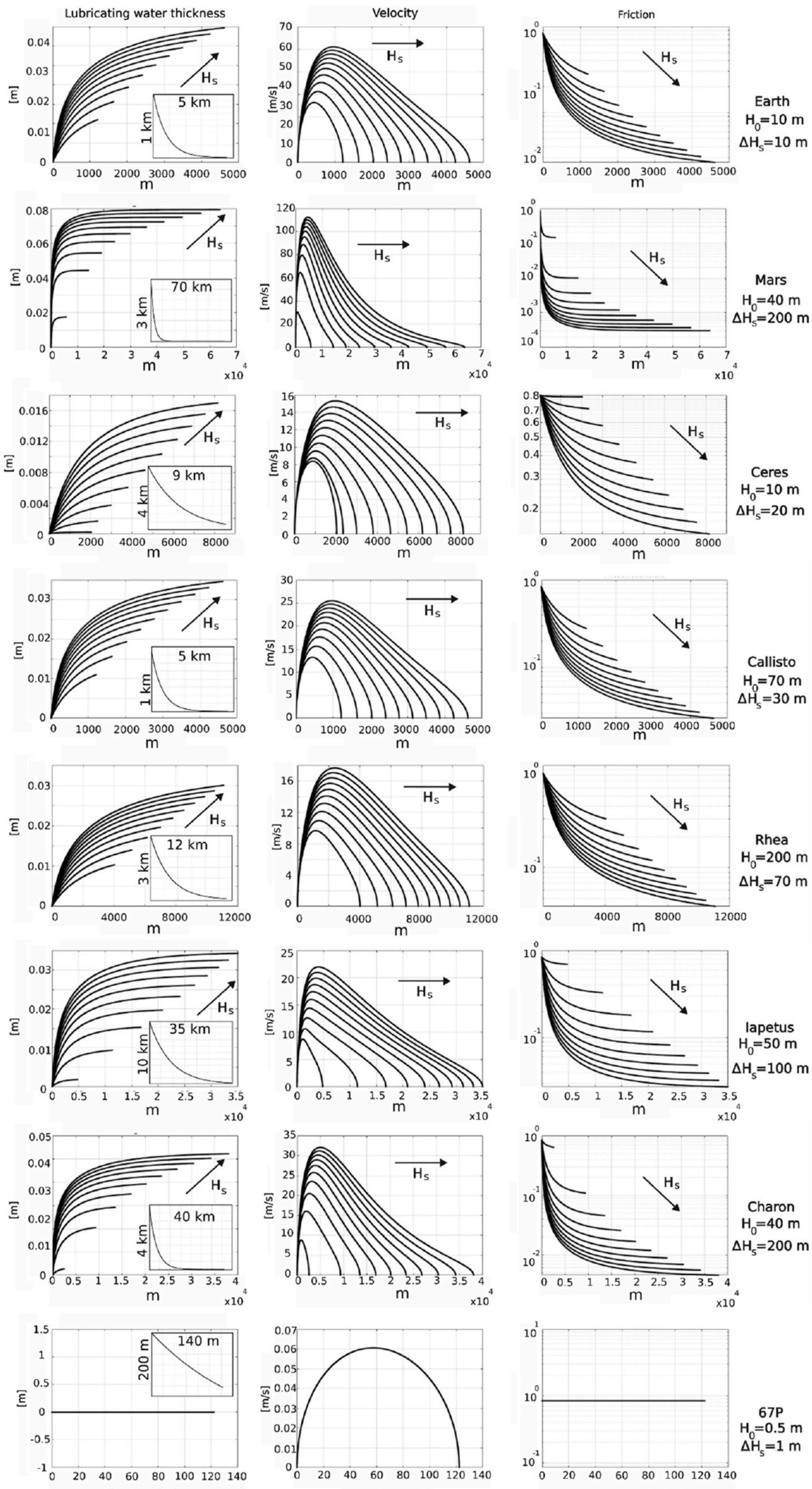

(caption on next page)

Fig. 4. Results of the simulations for Earth, Mars, Ceres, Callisto, Rhea, Iapetus, Charon, and Comet 67P Churyumov-Gerasimenko. The first column shows the relationship between the thickness of the lubricating water layer δ_w and the runout distance. In this column there are also the topographic profiles used for each simulation (see Supplementary Materials for a clearer representation); the second column shows the dependence between the velocity of the landslide and the runout distance; the third column shows the dependence between the friction coefficient and the runout distance. In each graph, the arrow shows the constant increase in the landslide thickness and each line is a single simulation with a different material height. Thus, the height is $H_f = H_0 + n\Delta H_s$, where n is the number of volume increases. and for each body the values were changed to match observations (see Supplementary Materials).

Table 3
Values of profile parameters for each planetary body and shown in the simulation results.

	Earth	Mars	Ceres	Callisto	Rhea	Iapetus	Charon	Comet 67P
y_0 (m)	1000	3000	4000	740	3000	10000	4000	200
Λ (m)	800	2700	3500	650	2700	8800	3500	170

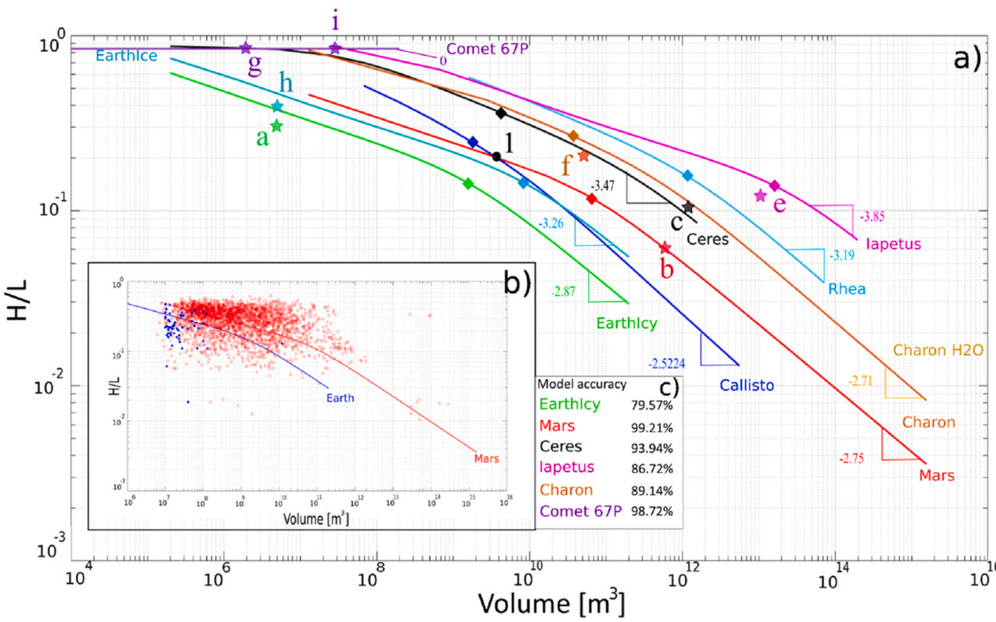

Fig. 5. H/L ratio versus volume plot. a) The plotted lines are the results of the simulations ran for the different planetary bodies. The letters, related to the stars, refer to the examples of Fig. 1 and show the agreement between the simulated data and the measured data, considering the wide spread of data evident in panel b. Measurements for Rhea and Callisto are not provided as no altimetric and volume data are available for these bodies. "i" was not portrayed in Fig. 1 and refers to landslide 20 in Lucchetti et al. (2019), the highest landslide volume measured on Comet 67P Churyumov/Gerasimenko. For each curve it is reported the α coefficient of the terminal part of the curve following the law $\frac{H}{L} = V^{\alpha}$. The coefficients for both Charon simulations are identical. The diamond markers indicate the positions of the "knees". b) The plotted lines are simulations ran for Earth and Mars. The dots are measured data for icy landslides (Sosio et al., 2012; Crosta et al., 2018b; Schneider et al., 2011). c) accuracy in percentage between the modeled curve and the measured data (portrayed as stars in panel a).

To explain such differences in the value of H/L, yet with similarities in the curve trend, we note that the most important difference between simulations is the general decrease in the gravitational acceleration of the celestial body towards the upper right section of Fig. 5a. This results in a decrease in pressure applied at the base of the landslide which results in a lower friction and therefore the release of a lower amount of energy capable of creating a thinner layer of meltwater at the base of the landslide, ultimately decreasing the H/L values.

The second driving factor defining these morphologies that emerges from this graph is the ice fraction (ϵ) present in the landslide material. This is evident when observing the data relative to "Earth-Icy" ($\epsilon = 0.2$) and "Earth-Ice" ($\epsilon = 0.8$).

The relationship between ice volume fraction ε and landslide mobility shows a counter-intuitive behavior that deserves explicit discussion. Across all simulated planetary bodies, an increase in ε produces higher H/L values (i.e. a lower runout efficiency) at a given landslide volume (Fig. 5a). This result appears to contradict the expectation that a higher proportion of ice should facilitate greater mobility through more efficient basal melting. However, the dominant control in the model is not the absolute availability of ice, but the basal pressure generated by the sliding mass. At low ε (rock-dominated mixture), the bulk density $\rho_{mix} = \varepsilon\ \rho_{ice} + (1-\varepsilon)\ \rho_{rock}$ is significantly higher, approaching $\rho_{rock} \approx 2700$ kg/m^3. This high density produces a proportionally larger basal pressure $P = \rho_{mix}\, g\, H_s \cos\beta$, which in turn generates more frictional heat for a given slab thickness and slope. In the present formulation, the energy denominator $\rho_{water}\,(c_{ice} \cdot \Delta T + \lambda_{ice})$ is independent of ε, so the sole physical mechanism is the reduction of basal pressure through the decrease of ρ_mix with increasing ice content. Over the range ε = 0.2 to 0.8, ρ_{mix} decreases from ~2343 to ~1274 kg m^{-3} (factor ~1.8), directly reducing the frictional heating rate and therefore the water-film growth rate by the same factor. This single, physically transparent mechanism fully accounts for the counterintuitive increase of H/L with ε.

Because the available ice fraction, although smaller, is sufficient to form a lubricating layer under these conditions, the net effect is a thicker water film δ_w and a lower effective friction coefficient μ than achieved by a lighter, ice-dominated slab of equivalent volume. At high ε, the lower mixture density reduces the basal pressure, limiting heat generation despite the larger ice reservoir. This pressure-driven mechanism explains why icy landslides with moderate rock content (ε ≈ 0.2–0.4) can achieve lower H/L values than nearly pure ice masses (ε ≈ 0.8–0.99) of the same volume. This is consistent with the observation that Martian rock-ice debris aprons show systematically lower apparent friction than the nearly pure-ice avalanches of Iapetus and Rhea (Singer et al., 2012; Crosta et al., 2018a). Additional information on the impact of ε on H/L in the Supplementary Materials.

An interesting case in this regard is presented by the results of Callisto ($\epsilon = 0.4$) and Mars ($\epsilon = 0.2$).

Fig. 5a shows how, at low landslide volumes, Callisto exhibits higher H/L values than Mars. However, when the volumes exceed roughly $3.5\times 10^9 m^3$ (point 1 in Fig. 4a), we observe a change in the trend with Callisto's H/L values becoming much lower than Mars' ones. We interpreted this behavior as resulting from the reaching of a critical mass value on Callisto that, combined with its moderate gravity $g = 1.235\, m/\, s^2$, could generate a significant amount of heat. When this heat meets the ice-rich composition of Callisto (≈ 50% ice in surface composition; Moore et al., 2004), it melts relatively larger quantities of ice with respect to Mars (varying ice in surface composition, up to 20%; Taylor, 2013) that, together with its lower g, would result in a much larger decrease in H/L.

It is also interesting to note the low influence of the difference between the average temperature of the planetary body and the melting temperature of water , ΔT. Despite the low temperatures in the external bodies of the solar system, the role of the initial temperature turns out to be negligible as evident when comparing the result for Iapetus with the ones for Rhea. In our simulations, the two moons have the main controlling factors, i.e., gravity and ice content, almost equal (Iapetus $g = 0.22\, m/s^2$ and $\epsilon = 0.95$ while Rhea $g = 0.26\, m/s^2$ and $\epsilon = 0.95$). The temperature difference ΔT between the surficial T and 0K on these bodies is more significant, approximately 170 K for Iapetus and 197K for Rhea. Nonetheless, the simulation shows that Rhea, with a slightly higher gravity field, exhibits values of H/L lower than the ones for Iapetus, showing the dominance of g (and therefore pressure) over surface T conditions. Further evidence for the low dependence on ΔT is given by the case of Charon. Fig. 5a shows two labels “Charon” and “Charon H_2O”, which correspond to two separate simulations for the case of Charon that superimpose. These two simulations have been conducted with a composition similar to the one of Charon (roughly 30% ammonia ice and 70% water ice, Protopapa et al., 2021) and a pure water ice (100% water ice), respectively. The major difference in these simulations is the melting point T that, at 1 atm, decreases from 273 K of pure ice to roughly 190 K of the ice-ammonia mixture (Hogenboom et al., 1997). In the figure, it is possible to appreciate how such a major change in melting Temperature ($\Delta T = 83$K) causes a negligible decrease in H/L values (further discussion on T dependence in Supplementary Materials). Note that pressure, a major factor in defining ice melting behavior, is 0 atm on the surface of Charon, and other moons analyzed; therefore, in the simulations it solely depends on the volume of mass displaced, which is the same for both simulations. This allowed us to evaluate the impact of ice composition in lubricating landslides.

We interpret this behavior as the result of the large volumes of materials involved in the landslides: the amount of frictional energy dissipated and basal pressure applied is in fact so large that it is capable of melting large quantities of ice almost regardless of the initial temperature and pressure of the body. A very interesting aspect is that the results for the comet show high and constant H/L values, regardless of the ice volumes involved (e.g. Comet 67P/Churyumov-Gerasimenko, $g = 0.00022\, m/s^2$ and H/L ≈ 0.85). This is in line with data (Lucchetti et al., 2019), and has an explanation in the low amount of energy generated by landslides occurring on a celestial body with extremely low gravity. This results in the absence of the lubricating water layer (Fig. 4, Comet results), indicating the important role of gravitational acceleration in ice melting and explains the absence of volume effect on the surface of the comet (Lucchetti et al., 2019). On this body, processes of volatile sublimation (e.g. CO, CO_2, NH_3, CH_4, Filacchione et al., 2019a,b) could have a major impact than basal melting. Although these processes may not be large enough to cause basal lubrication, they may play a major role as landslide triggers.

The pressure dependence of the ice melting point, described by the Clausius-Clapeyron relation $dT/dP = -7.4 \times 10^{-8}$ K/Pa (Petrenko and Whitworth, 1999), introduces a positive feedback between slab thickness and basal melting efficiency. A thicker slab generates a higher lithostatic pressure $P = \rho_{mix}\, g\, H_s \cos\beta$, which depresses the melting point by $\Delta T_{CC} = |dT/dP|\ P$, thereby reducing the temperature gap $\Delta T = T_{melt} - T_{surf}$ that must be overcome before melting begins. To assess the importance of this correction, we implemented a spatially varying T_{melt_eff} recomputed at each integration step as the slope angle evolves along the profile. Results indicate that this effect is negligible for all planetary bodies investigated here (see Supplementary Materials for the visual representation of this effect). For the largest Martian landslides modeled ($H_s = 5000$ m), $\Delta T_{CC} \approx$ 2-3 K compared to a nominal $\Delta T_{base} = 50$ K, representing a reduction of ∼4-6% in the energy required for melting. The corresponding change in H/L is less than 0.5%, well within the noise of the empirical scatter in observed data. For external solar system bodies with $g \leq 0.3$ m/s^2, ΔT_{CC} remains below 0.5 K across the entire physically plausible range of slab thicknesses, completely negligible relative to ΔT_{base} values of 100–220 K. The Clausius-Clapeyron threshold of 10% of ΔT_{base} is only reached for Mars at slab thicknesses exceeding ∼8000–10,000 m, well beyond any documented individual landslide deposit. These results are consistent with, and further quantify, the conclusion that initial temperature plays a secondary role in controlling basal lubrication dynamics across the Solar System. Thus, the Clausius-Clapeyron correction does not alter any of the conclusions presented here (visual representation of this effect in the Supplementary Materials).

4.3. Model accuracy assessment

To assess the accuracy of our model, we gathered several data taken from landslide measurements on Earth (blue) and Mars (red) and plotted them as single points in Fig. 5b superimposed to our simulations for Earth and Mars. We chose these two planets as they are the ones with larger landslide databases; the data was taken from Schneider et al. (2011), Sosio et al. (2012) and Crosta et al. (2018b). What emerges from Fig. 5b is that the model can reproduce the general trend of landslide evolution for the chosen bodies. The results are particularly promising for the case of Mars, where the large volumes of material involved in landslides allowed us to test the model on a wider range of data (up to $10^{14} - 10^{15}\ m^3$). For the case of Earth, the quality of our simulations could only be assessed for lower volumes, as icy landslides on Earth are scarce and generally involve restricted volumes of material.

Within the context of Fig. 5b, we quantified the agreement between the observed datasets and our modeled curves by computing the Root Mean Squared Perpendicular Distance (RMSPD). Specifically, the fit quality was evaluated as the root mean square of the perpendicular distances between each landslide data point and our simulation as a fixed reference line. To assess statistical significance, we implemented a Monte Carlo hypothesis test in which synthetic datasets were generated under a null model assuming Gaussian-distributed scatter around the reference line, with variance estimated from the observed residuals. For each synthetic realization, the RMSPD was recomputed, allowing us to estimate a p-value as the fraction of simulations exhibiting equal or greater deviation than the observed data. The results show that the Earth dataset yields RMSPD = 0.258 with $p = 0.0006$. This low p-value is the consequence of the large scattering of data, which reflects the high heterogeneity of icy landslides on Earth. The Mars dataset, on the other hand, yields RMSPD = 0.222 with $p = 0.367$, consistent with the null model and suggesting that the proposed scaling relationship adequately describes the Martian data within the assumed noise structure.

Additionally, the model assumed a constant thickness and no deformation. However, rock avalanches deform during the flow as consequence of fragmentation and differential pull of some of its parts

(Nicoletti and Sorriso-Valvo, 1991). Clearly, deformation changes the thickness of a landslide thus modifying the pressure distribution and the basal ice melting rate and spread. Even though it would be possible to partially account for this effect in a deforming model, we preferred to keep a simple view that would be broken by introducing more assumptions that require sufficiently precise modelling.

Lastly, the model includes water loss from the tail of the slab but not lateral and frontal refreezing. For bodies like Charon (53 K), Rhea (76 K), or Iapetus (100 K), the meltwater would recrystallize almost instantaneously at the margins of the slab. This process would limit lubrication more effectively than simple water loss from the tail. Its omission could lead to an overestimation of the lubrication on these bodies.

4.4. Previous works

Parekh et al. (2021) investigated the volume effect for numerous mass movements on non-icy Vesta ($g = 0.22\,ms^{-2}$) and (icy) Ceres of slightly higher gravity ($g = 0.28\,ms^{-2}$). They found only a small volume effect for the former, and a stronger one for Ceres, but the plot is presented in terms of either landslide length or width, which are only proxies of the volume. Despite this caveat, and noting the similar gravity of the two bodies, this observation may be in line with the present model. If, as suggested by Scully et al. (2015); Stubbs and Wang (2012), ice is present on Vesta, the different slope of the H/L versus volume from Vesta and Ceres may be due to the different gravity. If, however, ice is absent on Vesta, the residual volume effect may be due to one of the several explanations that have been put forward that do not involve any lubricating medium or phase transformations (e.g., Korup et al., 2013). As a partial selection, we mention the work by Melosh (1979) and Collins and Melosh (2003) who suggest that high-frequency acoustic oscillations by the highly energetic movement of the landslide may diminish particle interaction, thus reducing effective friction. Campbell (1989) and Cleary and Campbell (1993) envisage the volume effect as resulting from the dynamics of particle-particle interactions without the need for a lubricating medium. We also mention for completeness that explanations based on media other than ice have been considered such as molten rock (Erismann, 1979), high-temperature generation of gases (Habib, 1975), or water (Legros, 2002; De Blasio, 2009).

Additionally, the results of this work are also in accordance with the study conducted by Lucas et al. (2014), where the increase in landslide velocity and landslide volume was related to the decrease in effective friction coefficient. The simulations reported here found a similar trend, showing the relationship between velocity, volume and friction coefficient values. The good agreement between the results therefore shows that gravity, water-ice content and temperature strongly influence the final morphologies of landslides, and that, as hypothesized by Lucas et al. (2014), flash heating-caused basal melting at different scales should be taken into consideration when studying and modelling the behavior of icy landslides.

5. Conclusion

This work investigated the importance of the volume effect in the effective friction coefficient of landslides occurring on planetary bodies with varying amounts of surficial ice. Calculations were performed using a mathematical model for landslides simulated as rigid slabs, generating heat at their base through friction. This heat would be partially used to melt some of the water ice present in the falling material and in the subsurface, thus creating a layer of liquid water at the base of the landslide. On an icy body, this layer would then be able to lubricate the mass movement, resulting in the low apparent friction coefficient (H/L) values that are measured via satellite data.

A total of eight planetary bodies with varying amounts of ice in their composition (Earth, Mars, Ceres, Callisto, Rhea, Iapetus, Charon and Comet 67P Churyumov-Gerasimenko) were examined, finding that the pressure applied by the landslide (directly dependent on the g of the body) had a major role in determining the runout of the landslides. Bodies with extremely low gravity, in fact, exhibited high H/L values, regardless of their ice volume fractions, with a complete lack of the volume effect for Comet 67P Churyumov-Gerasimenko ($g = 0.00022\,m/s^2$; $\Delta T = 170K$ and H/L ≈ 0.85), while larger bodies showed very low H/L values even with lower ice fractions in their composition (e.g. Earth, $g = 9.81\frac{m^2}{s}$; $\Delta T = 10K$ and H/L $\approx$ 0.2-0.3). Hence, basal lubrication via frictional melting of water ice is likely to occur in landslides on icy bodies and plays a major role in shaping the final morphologies that these landslides assume throughout the Solar System.

This model could also provide indirect estimations of the bulk surface ice content and thickness of the interface liquid water layer during landslides on the surfaces of icy planetary bodies based on the aspect ratio (H/L). Such insight, paired with additional measurements (i.e. spectral and radar data), would prove extremely useful in understanding the properties of the icy surfaces of remote planetary bodies with poor data coverage. In fact, the model requires satellite images with high enough resolution to estimate the geometrical properties of the landslide deposit (of order 1 km/pixel for the largest landslides would suffice).

Better data and understanding of the landslide dynamics will bring significant contributions to this model with the ultimate aim of a better understanding of the behavior of icy materials throughout the Solar System.

CRediT authorship contribution statement

Andrea Caccia: Conceptualization, Data curation, Formal analysis, Methodology, Validation, Visualization, Writing – original draft, Writing – review & editing. **Fabio V. De Blasio:** Conceptualization, Data curation, Methodology, Software, Supervision, Writing – review & editing. **Ludovica Dalla Costa:** Data curation, Investigation, Validation. **Biagio Di Mauro:** Validation, Writing – review & editing. **Giovanni B. Crosta:** Conceptualization, Methodology, Visualization, Writing – review & editing.

Declaration of competing interest

The authors declare that they have no known competing financial interests or personal relationships that could have appeared to influence the work reported in this paper.

Appendix A. Supplementary data

Supplementary data to this article can be found online at https://doi.org/10.1016/j.pss.2026.106295.

Data availability

Data will be made available on request.

References

Anderson, J.D., Jacobson, R.A., McElrath, T.P., Moore, W.B., Schubert, G., Thomas, P.C., 2001. Shape, mean radius, gravity field, and interior structure of callisto. Icarus 153 (1), 157–161.
Anderson, J.D., Schubert, G., 2007. Saturn's satellite rhea is a homogeneous mix of rock and ice. Geophys. Res. Lett. 34 (2).
Anesio, A.M., Lutz, S., Chrismas, N.A., Benning, L.G., 2017. The microbiome of glaciers and ice sheets. npj Biofilms Microbiomes 3 (1), 10.
Beddingfield, C.B., Beyer, R.A., Singer, K., Nimmo, F., McKinnon, W.B., Moore, J.M., et al., 2018. Landslides in the serenity Chasma region, charon. 49th lunar planet. Sci abs. #2083.
Beddingfield, C.B., Beyer, R.A., Singer, K.N., McKinnon, W.B., Runyon, K., Grundy, W., et al., 2020. Landslides on charon. Icarus 335, 113383.
Brunetti, M.T., Xiao, Z., Komatsu, G., Peruccacci, S., Guzzetti, F., 2015. Large rock slides in impact craters on the moon and mercury. Icarus 260, 289–300.

Bulmer, M.H., 2012. Landslides on other planets. Landslides: Types, Mechanisms and Modeling. Cambridge Univ Press, Cambridge, pp. 393–408.
Campbell, C.S., 1989. Self-lubrication for long runout landslides. J. Geol. 97 (6), 653–665.
Christensen, P.R., Engle, E., Anwar, S., Dickenshied, S., Noss, D., Gorelick, N., Weiss-Malik, M., 2009. JMARS-a planetary GIS. In: AGU Fall Meeting Abstracts, 2009. IN22A-06.
Clark, R.N., Cruikshank, D.P., Jaumann, R., Brown, R.H., Stephan, K., Dalle Ore, C.M., et al., 2012. The surface composition of iapetus: mapping results from Cassini VIMS. Icarus 218 (2), 831–860.
Cleary, P.W., Campbell, C.S., 1993. Self-lubrication for long runout landslides: examination by computer simulation. J. Geophys. Res. Solid Earth 98 (B12), 21911–21924.
Colbeck, S.C., 1988. The kinetic friction of snow. J. Glaciol. 34 (116), 78–86.
Colbeck, S.C., 1995. Pressure melting and ice skating. Am. J. Phys. 63 (10), 888–890.
Collins, G.S., Melosh, H.J., 2003. Acoustic fluidization and the extraordinary mobility of sturzstroms. J. Geophys. Res. Solid Earth 108 (B10).
Crosta, G.B., De Blasio, F.V., Frattini, P., 2018a. Global scale analysis of Martian landslide mobility and paleoenvironmental clues. J. Geophys. Res. Planets 123 (4), 872–891.
Crosta, G.B., Frattini, P., Valbuzzi, E., De Blasio, F.V., 2018b. Introducing a new inventory of large Martian landslides. Earth Space Sci. 5 (4), 89–119. https://doi.org/10.1002/2017EA000324.
De Blasio, F.V., 2009. Rheology of a wet, fragmenting granular flow and the riddle of the anomalous friction of large rock avalanches. Granul. Matter 11 (3), 179–184.
De Blasio, F.V., 2014. Friction and dynamics of rock avalanches travelling on glaciers. Geomorphology 213, 88–98.
De Blasio, F.V., Dattola, G., Crosta, G.B., 2018. Extremely energetic rockfalls. J. Geophys. Res. Earth Surf. 123 (10), 2392–2421.
Encrenaz, T., 2008. Water in the solar system. Annu. Rev. Astron. Astrophys. 46 (1), 57–87.
Erismann, T.H., 1979. Mechanisms of large landslides. Rock Mech. 12, 15–46.
Filacchione, G., Groussin, O., Herny, C., Kappel, D., Mottola, S., Oklay, N., et al., 2019a. Comet 67P/CG nucleus composition and comparison to other comets. Space Sci. Rev. 215, 1–46.
Filacchione, G., Groussin, O., Herny, C., Kappel, D., Mottola, S., Oklay, N., et al., 2019b. Comet 67P/CG nucleus composition and comparison to other comets. Space Sci. Rev. 215 (1), 19.
Guimpier, A., Conway, S.J., Pajola, M., Lucchetti, A., Simioni, E., Re, C., et al., 2022. Pre-landslide topographic reconstruction in baetis chaos, mars using a CaSSIS digital elevation model. Planet. Space Sci. 218, 105505.
Guo, Y., Farquhar, R.W., 2008. New Horizons mission design. Space Sci. Rev. 140, 49–74.
Habib, P., 1975. Production of gaseous pore pressure during rock slides. Rock Mech. Rock Eng. 7 (4), 193–197.
Heim, A.: Der Bergsturz von Elm, Zeitschrift Der Deutschen Geologischen Gesellschaft, 34, 74–115, Schweizerbart Science Publishers, Stuttgart, Germany, 1882.
Hogenboom, D.L., Kargel, J.S., Consolmagno, G.J., Holden, T.C., Lee, L., Buyyounouski, M., 1997. The ammonia–water system and the chemical differentiation of icy satellites. Icarus 128 (1), 171–180.
Khuller, A.R., Warren, S.G., Christensen, P.R., Clow, G.D., 2024. Potential for photosynthesis on Mars within snow and ice. Commun. Earth Environ. 5 (1), 583.
Kietzig, A.M., Hatzikiriakos, S.G., Englezos, P., 2010. Physics of ice friction. J. Appl. Phys. 107 (8).
King, S.D., Castillo-Rogez, J.C., Toplis, M.J., Bland, M.T., Raymond, C.A., Russell, C.T., 2018. Ceres internal structure from geophysical constraints. Meteorit. Planet. Sci. 53 (9), 1999–2007.
Korup, O., Schneider, D., Huggel, C., Dufresne, A., Shroder, J.F., 2013. 7.18 long-runout Landslides.
Lebreton, J.P., Matson, D.L., 1992. An overview of the Cassini mission. Il Nuovo Cimento C 15, 1137–1147.
Legros, F., 2002. The mobility of long-runout landslides. Eng. Geol. 63 (3- 4), 301–331.
Li, L., Lan, H., Strom, A., Macciotta, R., 2022. Landslide longitudinal shape: a new concept for complementing landslide aspect ratio. Landslides 19 (5), 1143–1163.
Lucas, A., Mangeney, A., Ampuero, J.P., 2014. Frictional velocity-weakening in landslides on Earth and on other planetary bodies. Nat. Commun. 5.
Lucchetti, A., Penasa, L., Pajola, M., Massironi, M., Brunetti, M.T., Cremonese, G., et al., 2019. The rocky-like behavior of cometary landslides on 67P/Churyumov-Gerasimenko. Geophys. Res. Lett. 46 (24), 14336–14346.
Lucchitta, B.K., 1987. Valles marineris, Mars wet debris flows and ground ice. Icarus 72, 411–429.
Maeno, N., Arakawa, M., Yasutome, A., Mizukami, N., Kanazawa, S., 2003. Ice friction measurements, and water lubrication and adhesion-shear mechanisms. Can. J. Phys. 81 (1–2), 241–249.
Malin, M.C., 1992. Mass movements on Venus: preliminary results from Magellan cycle 1 observations. J. Geophys. Res. Planets 97 (E10), 16337–16352.
McCord, T.B., Sotin, C., 2005. Ceres: evolution and current state. J. Geophys. Res. Planets 110 (E5).
McDonough, W.F., Sun, S.S., 1995. The composition of the Earth. Chem. Geol. 120 (3–4), 223–253.
McEwen, A.S., 1989. Mobility of large rock avalanches: evidence from valles marineris. Mars. Geology 17, 1111–1114.
Melosh, H.J., 1979. Acoustic fluidization: a new geologic process? J. Geophys. Res. Solid Earth 84 (B13), 7513–7520.
Moore, J.M., Asphaug, E., Morrison, D., Spencer, J.R., Chapman, C.R., Bierhaus, B., et al., 1999. Mass movement and landform degradation on the icy Galilean satellites: results of the galileo nominal mission. Icarus 140 (2), 294–312. https://doi.org/10.1006/icar.1999.6132.
Moore, J.M., Chapman, C.R., Bierhaus, E.B., Greeley, R., Chuang, F.C., Klemaszewski, J., et al., 2004. Callisto. Jupiter. The planet, satellites and magnetosphere 1, 397–426.
Nicoletti, P.G., Sorriso-Valvo, M., 1991. Geomorphic controls of the shape and mobility of rock avalanches. Geol. Soc. Am. Bull. 103 (10), 1365–1373.
Otto, K.A., Jaumann, R., Krohn, K., Matz, K.-D., Preusker, F., Roatsch, T., et al., 2013. Mass-wasting features and processes in Vesta's south polar basin Rheasilvia. J. Geophys. Res. Planets 118, 2279–2294. https://doi.org/10.1002/2013JE004333.
Pajola, M., Mergili, M., Cambianica, P., Lucchetti, A., Brunetti, M.T., Guimpier, A., et al., 2022. Modelling reconstruction and boulder size-frequency distribution of a young (< 5 Myr) landslide located in simud vallis floor, Mars. Icarus 375, 114850.
Parekh, R., Otto, K.A., Jaumann, R., Matz, K.D., Roatsch, T., Kersten, E., et al., 2021. Influence of volatiles on mass wasting processes on Vesta and Ceres. J. Geophys. Res. Planets 126 (3), e2020JE006573.
Petrenko, V.F., Whitworth, R.W., 1999. Physics of Ice. Oxford.
Protopapa, S., Cook, J.C., Grundy, W.M., Cruikshank, D.P., Dalle Ore, C.M., Beyer, R.A., 2021. Surface composition of charon. The Pluto System After New Horizons, pp. 433–456.
Pätzold, M., Andert, T., Hahn, M., Asmar, S.W., Barriot, J.P., Bird, M.K., et al., 2016. A homogeneous nucleus for comet 67P/Churyumov–Gerasimenko from its gravity field. Nature 530 (7588), 63–65.
Quantin, C., Allemand, P., Delacourt, C., 2004. Morphology and geometry of Valles marineris landslides. Planet. Space Sci. 52, 1011–1022.
Rivkin, A.S., Li, J.Y., Milliken, R.E., Lim, L.F., Lovell, A.J., Schmidt, B.E., et al., 2012. The surface composition of ceres. The Dawn Mission to Minor Planets 4 Vesta and 1 Ceres 95–116.
Rozwalak, P., Podkowa, P., Buda, J., Niedzielski, P., Kawecki, S., Ambrosini, R., et al., 2022. Cryoconite–From minerals and organic matter to bioengineered sediments on glacier's surfaces. Sci. Total Environ. 807, 150874.
Russell, C.T., Raymond, C.A., 2012. The Dawn Mission to Vesta and Ceres. Springer, New York, pp. 3–23.
Scaioni, M., Yordanov, V., Brunetti, M.T., Melis, M.T., Zinzi, A., Kang, Z., Giommi, P., 2018. Recognition of landslides in lunar impact craters. European Journal of Remote Sensing 51 (1), 47–61.
Scheidegger, A.E., 1973. On the prediction of the reach and velocity of catastrophic landslides. Rock Mech. Rock Eng. 5 (4), 231–236.
Scheidegger, A.E., 2012. Theoretical Geomorphology. Springer Science & Business Media.
Schenk, P.M., Bulmer, M.H., 1998. Origin of mountains on Io by thrust faulting and large-scale mass movements. Science 279 (5356), 1514–1517. https://doi.org/10.1126/science.279.5356.1514.
Schmidt, B.E., Hughson, K.H.G., Chilton, H.T., Scully, J.E.C., Platz, T., Nathues, A., et al., 2017. Geomorphological evidence for ground ice on dwarf planet ceres. Nat. Geosci. 10, 338–343.
Schneider, D., Huggel, C., Haeberli, W., Kaitna, R., 2011. Unraveling driving factors for large rock–ice avalanche mobility. Earth Surf. Process. Landf. 36 (14), 1948–1966.
Scully, J.E., Russell, C.T., Yin, A., Jaumann, R., Carey, E., Castillo-Rogez, J., et al., 2015. Geomorphological evidence for transient water flow on Vesta. Earth Planet Sci. Lett. 411, 151–163.
Shaller, P.J., 1991. Analysis of a large moist landslide, Lost river range, Idaho, USA. Can. Geotech. J. 28 (4), 584–600.
Shingareva, T.V., Kuzmin, R.O., 2001. Mass-wasting processes on the surface of phobos. Sol. Syst. Res. 35, 431–443.
Singer, Kelsi N., McKinnon, William B., Schenk, Paul M., Moore, Jeffery M., 2012. Massive ice avalanches on iapetus mobilized by friction reduction during flash heating. Nat. Geosci. 5 (8), 574–578.
Smith, D.E., Zuber, M.T., Solomon, S.C., Phillips, R.J., Head, J.W., Garvin, J.B., et al., 1999. The global topography of Mars and implications for surface evolution. Science 284 (5419), 1495–1503.
Sosio, R., Crosta, G.B., Chen, J.H., Hungr, O., 2012. Modelling rock avalanche propagation onto glaciers. Quat. Sci. Rev. 47, 23–40.
Spencer, J., Beyer, R.A., Robbins, S.J., Singer, K.N., Nimmo, F., 2021. The geology and geophysics of charon. The Pluto System After New Horizons 395–412.
Stubbs, T.J., Wang, Y., 2012. Illumination conditions at the asteroid 4 vesta: implications for the presence of water ice. Icarus 217 (1), 272–276.
Taylor, G.J., 2013. The bulk composition of Mars. Geochemistry 73 (4), 401–420.
Thomas, P.C., Burns, J.A., Helfenstein, P., Squyres, S., Veverka, J., Porco, C., Turtle, E.P., McEwen, A., Denke, T., Giese, B., Roatsch, T., Johnson, T.V., Jacobson, R.A., 2007. Shapes of the saturnian icy satellites and their significance. Icarus. https://doi.org/10.1016/j.icarus.2007.03.012 (in press).
Williamson, E.D., Adams, L.H., 1923. Density distribution in the Earth. J. Wash. Acad. Sci. 13 (19), 413–428.
Zurek, R.W., Smrekar, S.E., 2007. An overview of the Mars Reconnaissance Orbiter (MRO) science mission. J. Geophys. Res. Planets 112 (E5).